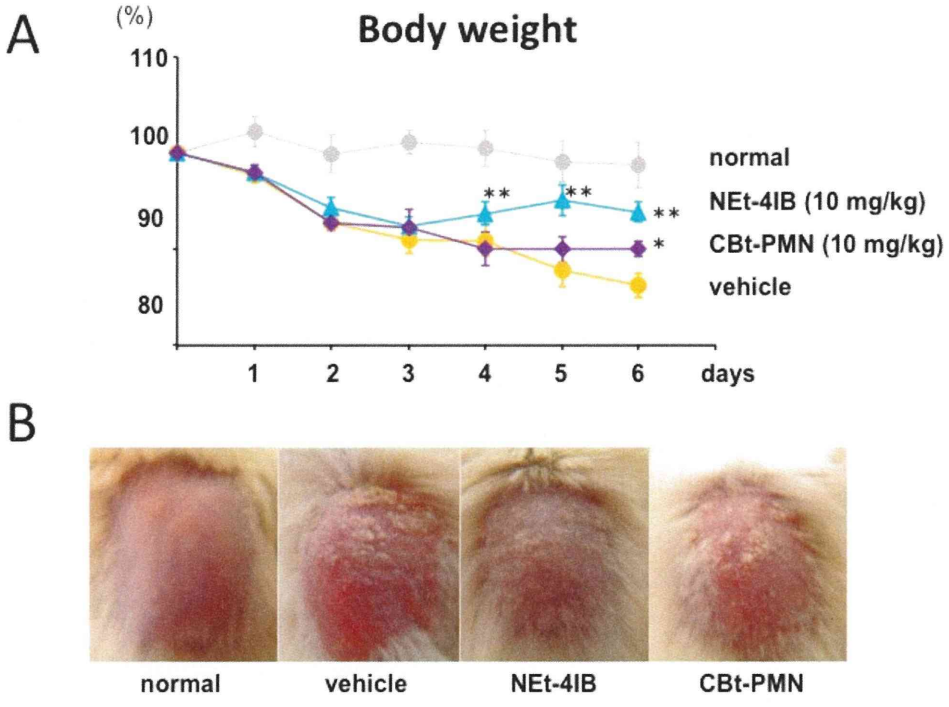

Figure 13. Imiquimod-induced skin inflammation in mice phenotypically resembles psoriasis. A) Body weight changes. B) Phenotypical presentation of mouse back skin after 6 days of treatment. Data shown are the average (n = 6) ± SEM and analyzed by one-way ANOVA followed by Bonferroni test. * : $p < 0.05$ and ** : $p < 0.01$ vs. vehicle respectively.

スト NEt-3IP および RXR パーシャルアゴニスト NEt-4IB 投与により，これらの発現が抑制もしくは抑制傾向を示した．一方で，Treg 誘導能かつ Th17 の発現抑制が報告されている RARα/βフルアゴニストである Am80[18] では，vehicle 群と変わらないことが分かった．

Treg 細胞（Foxp3$^+$発現 CD4$^+$細胞））については，NEt-3IP 投与群で上昇傾向が見られたが（Figure 12F），顕著なものではなかった．また，Am80 投与群における Treg 細胞は，vehicle 群に比べ低下した．

以上から，NEt-3IP および NEt-4IB による Th1 細胞（IFN-γ発現 CD4$^+$細胞），Th17 細胞（IL-17 発現 CD4$^+$細胞），Th1/17 細胞（IFN-γ/IL-17 発現 CD4$^+$細胞）の発現抑制作用は，Treg 誘導を介したものかは不明であり，今後の検討が必要である．

なお，組織切片，PCR 等による炎症性サイトカインの発現解析等を行うに至っていないため，引き続き本モデルでの有

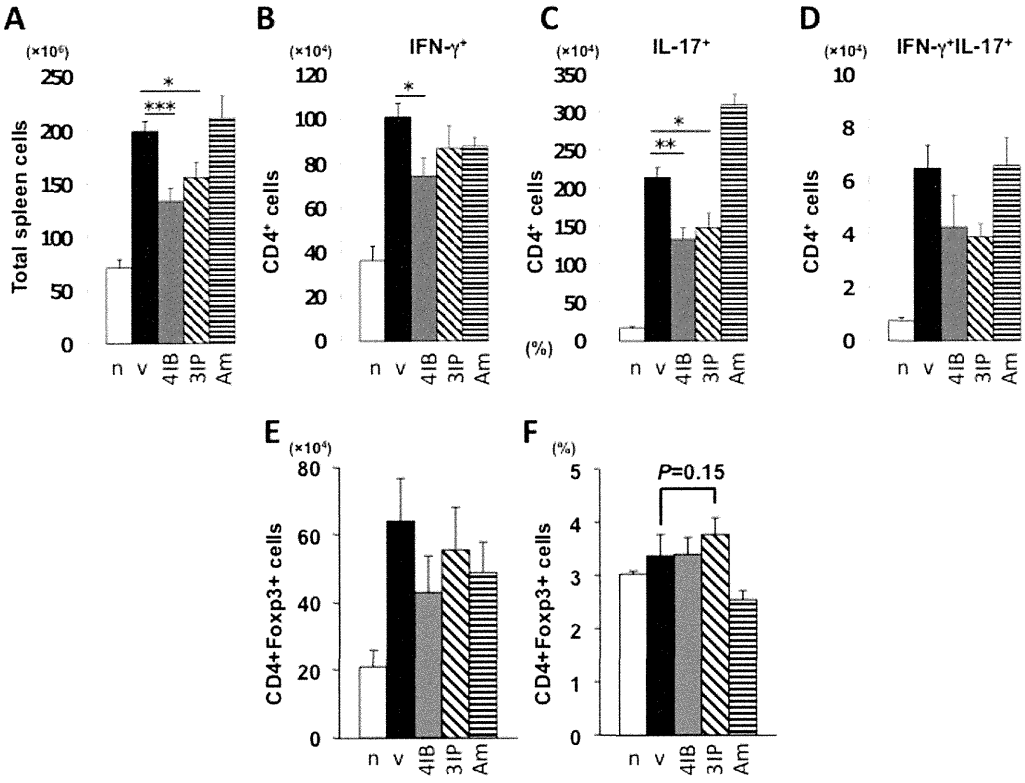

Figure 14. Topical imiquimod (IMQ) increases spleen mass and alters its cellular composition. Mice were treated with IMQ or control cream for 6 consecutive days. A, Mice were sacrificed and spleen total cells were determined. B–F, Spleen cells were analyzed for the cell numbers or percentage of T cells by flow cytometry. Data shown are the average (n = 5) ± SD and analyzed by t-test. * : $p < 0.05$, ** : $p < 0.01$ and *** : $p < 0.005$ vs. vehicle respectively.

効性を調べるべく，継続して実験を行う予定である．

【参考文献】

17. *Pediatric Research*, 2009, *65*, 26R–31R.

18. *Am. J. Pathol.* 2009, *174*, 2234–2245.

D. 考察

前年度において創出に成功した新規RXRパーシャルアゴニストCBTF-PMN(**4**)について，ラットへの28日間連続投与を行ったところ，フルアゴニストに比べて明らかに弱いものの，わずかな肝肥大が見られた．しかし，これまでのRXRフルアゴニストに見られた血中トリグリセリドの上昇は回避出来ており，なおかつ本化合物がTNBSモデルでも薬効を示したことから（前年度成果），RXRパーシャルアゴニストの有用性に期待がもたれた．

RXR パーシャルアゴニストの in vivo における報告は著者らの見出した CBt-PMN (**3**)および CBTF-PMN (**4**)に限られ，さらにこれらの化合物の分子構造は互いに類似

する．そこで，RXR パーシャルアゴニストであれば副作用を回避しつつ薬効を示すことの一般性を調べること，さらに本研究の目的とするクローン病や乾癬などの免疫疾患治療に有効な新たな小分子型医薬候補物質たるRXRパーシャルアゴニストの創出を目指し，新たなRXR パーシャルアゴニストの創出，その薬効・副作用発現について調べた．

合成した化合物の中でも疎水性部位 4’位にイソブトキシ基を有する化合物NEt-4IB (**11a**)に最もEC_{50}の小さいRXR パーシャルアゴニスト活性 (E_{max} = 55%, EC_{50} = 169 nM) を見出した．さらに，NEt-4IB (**11a**)を 30 mg/kg で経口投与し，血中移行性を調べたところ，良好な血中移行性 (C_{max} = 13.2 μM) を示すことが分かった．

このように新規RXRパーシャルアゴニストNEt-4IB (**11a**)を見出したことから，本化合物の副作用発現を調べた結果，マウスへの1週間連続投与，ラットへの28日間連続投与いずれにおいてもRXRフルアゴニストに見られるような体重増加，肝肥大，および血中TG値の上昇などの副作用は見られなかった．また，4-chloro-7-nitro-2,1,3-benzoxadiazole (NBD-Cl) 溶液を腸注することでクローン病モデルマウスを作成し，化合物の投与を行うことで薬効である抗炎症作用の評価を行ったところ，NEt-4IB (**11a**)の投与によって体重や腸長の改善が見られた．大腸のPCRを行い，炎症性サイトカインの発現を調べた結果，IL-1βやIL-6の顕著な低減が見られ，NEt-4IB (**11a**)の抗炎症作用が示された．さらに，imiquimodによる乾癬モデルを作成し，これにおいても有効なことを確認した．なおこれらの成果は，新たな特許出願に至っている（特願2012-224474）．

E. 結論

本研究により，研究当初に取り扱っていたRXRパーシャルアゴニストCBt-PMN (**3**)より顕著な薬効を示しながら，RXRフルアゴニストに見られる副作用発現を回避した新規RXRパーシャルアゴニストNEt-4IB (**11a**)の発見に至った．さらに，NEt-4IB (**11a**)はCBt-PMN (**3**)と分子構造が明らかに異なりながら，クローン病モデルマウスでの有効性が示されたことから，RXRパーシャルアゴニストであれば一般的に副作用を回避しつつ薬効を示すことが示唆された．さらに，乾癬モデルマウスでの有効性も示唆された．

これまでRXRアゴニストは脂質代謝異常症やアルツハイマー病等にも有効性が報告されているが，その副作用発現が問題となっており，臨床応用はされていなかった．しかし，RXR パーシャルアゴニストであれば副作用が回避できることが示唆されたため，本研究を通じて見出された NEt-4IB (**11a**)，もしくはその他のRXR パーシャルアゴニストを今後精査す

ることで，本事業で対象とした自己免疫疾患に限らず，これまでにRXRフルアゴニストで報告のある糖尿病，脂質異常症，およびアルツハイマー病などに対する新薬候補としても期待がもたれる．

本事業と別途，CBt-PMN(**3**)およびNEt-4IB (**11a**)についてOECD準拠によるAmes 試験を岡山大学大学院医歯薬学総合研究科 有元佐賀恵准教授により行って頂いた．その結果，対象とした5菌株に対しいずれも陰性であり，変異原性は認められなかった．

なお，これらの成果に関する知財をもとにした共同研究について，企業等との協議を展開中である．

F. 研究発表

1．論文発表

Ohsawa F, Yamada S, Yakushiji N, Shinozaki R, Nakayama M, Kawata K, Hagaya M, Kobayashi T, Kohara K, Furusawa Y, Fujiwara C, Ohta Y, Makishima M, Naitou H, Tai A, Yoshikawa Y, Yasui H, Kakuta H*. Mechanism of Retinoid X Receptor Partial Agonistic Action of 1-(3,5,5,8,8-Pentamethyl-5,6,7,8-tetrahydro-2-naphthyl)-1*H*-benzotriazole-5-carboxylic Acid and Structural Development To Increase Potency. *J. Med. Chem.*, 2013, *56*, 1865−77.

2．学会発表

川田 浩平，中山 真理子，森下 健一，大澤 史宜，山田 翔也，小林 俊貴，槇島 誠，田井 章博，加来田 博貴，RXRフルアゴニストに見られる副作用を回避しつつ炎症性腸疾患を改善するRXRパーシャルアゴニストNEt-4IB，メディシナルケミストリーシンポジウム（東京）

川田 浩平，中山 真理子，森下 健一，大澤 史宜，山田 翔也，小林 俊貴，田井 章博，加来田 博貴，RXRパーシャルアゴニストNEt-4IBの創出と薬効・副作用評価，レチノイド研究会（米子）

G. 知的所有権の取得状況

名称：レチノイドX受容体パーシャルアゴニスト化合物及びこのレチノイドX受容体パーシャルアゴニスト化合物を有効成分として含有する薬剤，特願2012-224474，出願日：平成24年10月9日，発明者：加来田博貴，出願人：岡山大学

II. 分担研究報告

厚生労働科学研究費補助金　（創薬基盤推進研究事業）
分担研究報告

薬効評価を目的とする遺伝子等発現解析

研究分担者　大橋俊孝

岡山大学大学院医歯薬学総合研究科　分子医化学　准教授

研究要旨

本研究では，研究代表者により創出されたRXRパーシャルアゴニストNEt-4IBによるクローン病モデル動物における抗炎症作用を評価するために，PCRによる炎症性サイトカインの発現について調べた．その結果，本モデルの炎症誘発群においてIL-1βならびにIL-6の発現が有意に増強していること，またNEt-4IB投与により，これらの炎症性サイトカインの発現が有意に抑制されることが確認された．

A.　研究目的

研究代表者により創出されたRXRパーシャルアゴニストNEt-4IBによるクローン病モデル動物における抗炎症作用を評価するために，PCRによる炎症性サイトカインの発現について調べた

B.　研究方法

1）PCR実験

Fifty milligrams of colon tissue from Balb/c mice described above was resected and mechanically homogenized with a Politron PT 10/35 (Kinematica Inc., Littau-Luzern, Switzerland) in 0.5 mL of Trizol reagent (Invitrogen, Carlsbad, CA). Total RNA was extracted as previously described (reference 1). Quantitative real-time RT-PCR analysis was performed using a LightCycler rapid thermal cycler system (Roche Applied Science, Mannheim, Germany) following the protocol previously reported (reference 2). Two micrograms of total RNA was reverse-transcribed by random hexamer priming using ReverTra Ace (Toyobo, Osaka, Japan). The PCR mixture consisted of 1x SYBR Green PCR Master Mix (Toyobo), which includes DNA polymerase, SYBR Green I Dye, dNTPs, PCR buffer, 8.0 pmol forward and reverse primers and cDNA of samples in a total volume of 10 μL. The amplification of a housekeeping gene, β -actin, was used to normalize the efficiency of cDNA synthesis

Table 1. Primer list

Primer		Sequence
β-actin	Forward	5'-TGACAGGATGCAGAAGGAGA-3'
	Reverse	5'-GCTGGAAGGTGGACAGTGAG-3'
IL-1β	Forward	5'-TCCAGGATGAGGACATGAGCAC-3'
	Reverse	5'-GAACGTCACACACCAGCAGGTTA-3'
IL-6	Forward	5'-CCACTTCACAAGTCGGAGGCTTA-3'
	Reverse	5'-CCAGTTTGGTAGCATCCATCATTTC-3'
TNF-α	Forward	5'-TATGGCCCAGACCCTCACA-3'
	Reverse	5'-GGAGTAGACAAGGTACAACCCATC-3'

and the amount of RNA applied. PCR was performed with initial denaturation at 94°C for 30 sec, followed by amplification for 40 cycles, each cycle consisting of denaturation at 94°C for 30 sec, annealing at 58°C for 30 sec, and polymerization at 72°C for 40 sec.

【参考文献】

1. *Mol. Cell. Neurosci.*, 2003, *24*, 148–159.
2. *J. Comp. Neurol.*, 2012, *520*, 1721–1736.

2）統計学的処理

有意差検定は vehicle 群と薬物投与群との間は, Bonferroni の多重検定により行った.

C.　研究結果

解剖時に大腸を採取し，ホルマリンで固定し，切片の作成した．その結果をFigure 1に示す．炎症誘発群であるvehicleは明らかに組織形態がnomarl群に比べ破壊され，顕著な炎症状態が確認された．一方で，炎症誘発群にNEt-4IBを投与した群においては，normal群に匹敵する改善が見られた．

炎症性サイトカインとして知られるIL-1β, IL-6, TNF-αの測定を行ったところ，炎症誘発群であるvehicleにおいてIL-1β, IL-6の明らかな上昇が確認された．一方でNEt-4IB (**11a**) 投与群の大腸は，normal群に匹敵するまでに回復していることが確認できた．

D.　考察

RXRパーシャルアゴニストである NEt-4IB (**11a**) は，NBD-Cl誘発クローン病

モデルマウスにて, 炎症所見の改善が認められ, さらに本実験により炎症性サイトカインであるIL-1βやIL-6の発現を有意に抑制していると言える.

E. 結論

NBD-Cl誘発クローン病モデルマウスにおける薬効評価について, 切片ならびにPCRによる炎症性サイトカインの発現について調べた. その結果, 体重減少の改善や腸長の改善に加えて, 組織切片における炎症所見の改善が認められ, さらに本実験により炎症性サイトカインであるIL-1βやIL-6の発現を有意に抑制していることが判明した. 以上から, RXRパーシャルアゴニストであるNEt-4IB (**15a**) の抗炎症作用が確認された.

NEt-4IB (**15a**)は, RXRフルアゴニストで見られた副作用を示すことなく, クローン病に対する新たな治療薬候補としての期待が持てる. また, この成果はRXRパーシャルアゴニストという創薬手法の有用性を支持する.

F. 研究発表

なし

G. 知的所有権の取得状況

なし

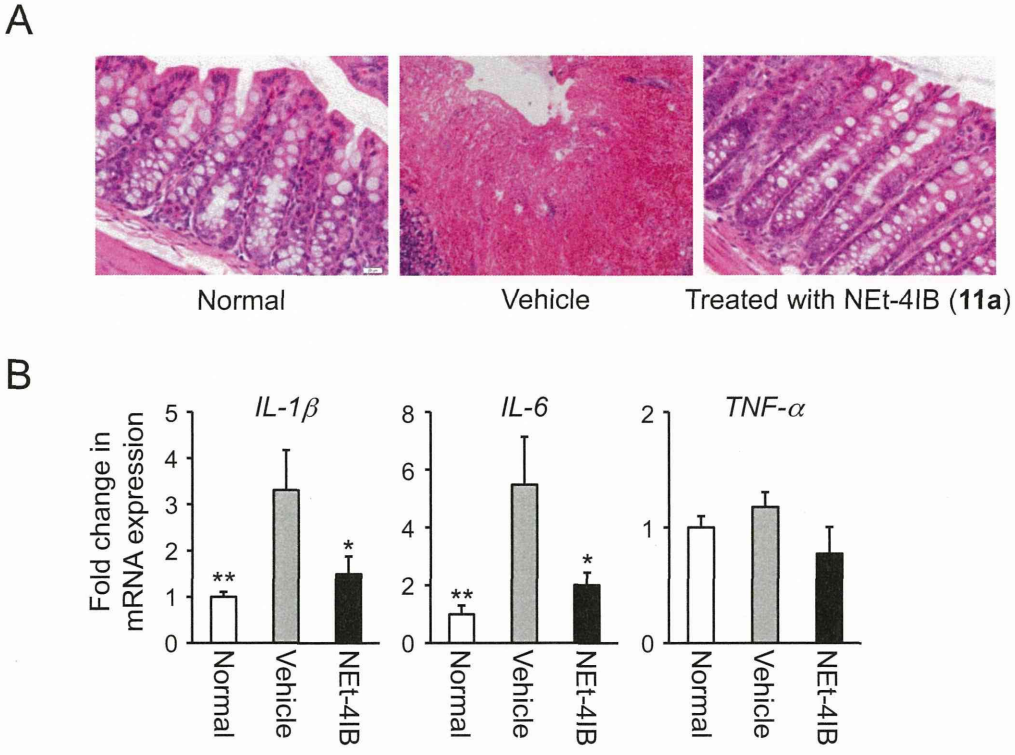

Figure 1. Anti-inflammatory effect of NEt-4IB (**11a**) in NBD-Cl induced inflammatory bowel disease model mice. A) Representative histological sections of colon tissues of Balb/c mice. B) Fold changes in mRNA expression of IL-1β, IL-6, and TNF-α in the colon tissue of normal mice or NBD-Cl induced bowel disease model mice treated with vehicle and NEt-4IB (**11a**) at 0.2 mg × 2/day for 4 consecutive days. 5. The white, gray, and black bars indicate normal, vehicle, and NEt-4IB (**11a**) treatment, respectively. Data shown are the average (n = 6-9) ± SEM and analyzed by one-way ANOVA followed by Bonferroni test. * : $p < 0.05$ and ** : $p < 0.01$ vs. vehicle respectively.

III. 研究成果を含む刊行物

研究成果の刊行に関する一覧表

雑誌

著者氏名	論文タイトル名	発表誌名	巻号	ページ	出版年
Fuminori Ohsawa, Shoya Yamada, Nobumasa Yakushiji, Ryosuke Shinozaki, Mariko Nakayama, Kohei Kawata, Manabu Hagaya, Toshiki Kobayashi, Kazutaka Kohara, Yuuki Furusawa, Chisa Fujiwara, Yui Ohta, Makoto Makishima, Hirotaka Naitou , Akihiro Tai , Yutaka Yoshikawa, Hiroyuki Yasui, and Hiroki Kakuta	Mechanism of Retinoid X Receptor Partial Agonistic Action of 1-(3,5,5,8,8-Pentamethyl-5,6,7,8-tetrahydro-2-naphthyl)-1H-benzotriazole-5-carboxylic Acid and Structural Development To Increase Potency	Journal of Medicinal Chemistry	56	1865–1877	2013

上記論文には，本事業にて行ったRXRパーシャルアゴニストCBTF-PMNのラット長期投与データを掲載している．なお，掲載箇所はSupporting information の**Figure S6**，**Figure S7**，**Table S1**，**Table S2**および**Table S4**である．次頁より本論文をそのまま掲載する．

Journal of Medicinal Chemistry

Article

pubs.acs.org/jmc

Mechanism of Retinoid X Receptor Partial Agonistic Action of 1-(3,5,5,8,8-Pentamethyl-5,6,7,8-tetrahydro-2-naphthyl)-1*H*-benzotriazole-5-carboxylic Acid and Structural Development To Increase Potency

Fuminori Ohsawa,[†] Shoya Yamada,[†,‡] Nobumasa Yakushiji,[†] Ryosuke Shinozaki,[†] Mariko Nakayama,[†] Kohei Kawata,[†] Manabu Hagaya,[†] Toshiki Kobayashi,[†] Kazutaka Kohara,[†] Yuuki Furusawa,[†] Chisa Fujiwara,[†] Yui Ohta,[†] Makoto Makishima,[§] Hirotaka Naitou,[∥] Akihiro Tai,[⊥] Yutaka Yoshikawa,[#] Hiroyuki Yasui,[#] and Hiroki Kakuta*[,†]

[†]Division of Pharmaceutical Sciences, Okayama University Graduate School of Medicine, Dentistry and Pharmaceutical Sciences, 1-1-1, Tsushima-Naka, Kita-Ku, Okayama 700-8530, Japan

[‡]Research Fellowship Division, Japan Society for the Promotion of Science, Sumitomo-Ichibancho FS Bldg., 8 Ichibancho, Chiyoda-ku, Tokyo 102-8472, Japan

[§]Division of Biochemistry, Department of Biomedical Sciences, Nihon University School of Medicine, 30-1 Oyaguchi-kamicho, Itabashi-ku, Tokyo 173-8610, Japan

[∥]Graduate School of Nutritional and Environmental Sciences, University of Shizuoka, 52-1 Yada, Suruga-ku, Shizuoka 422-8526, Japan

[⊥]Faculty of Life and Environmental Sciences, Prefectural University of Hiroshima, 562 Nanatsuka-Cho, Shobara, Hiroshima 727-0023, Japan

[#]Department of Analytical and Bioinorganic Chemistry, Division of Analytical and Physical Chemistry, Kyoto Pharmaceutical University, 5 Nakauchi-cho, Misasagi, Yamashina-ku, Kyoto 607-8414, Japan

Supporting Information

ABSTRACT: We have reported that retinoid X receptor (RXR) partial agonist 1-(3,5,5,8,8-pentamethyl-5,6,7,8-tetrahydro-2-naphthyl)-1*H*-benzotriazole-5-carboxylic acid (CBt-PMN, **4a**) shows a significant antidiabetes effect in the KK-A^y type 2 diabetes model mice, with reduced side effects compared to RXR full agonists. To elucidate the mechanism of the RXR partial agonist activity of **4a**, we synthesized derivatives of **4a**, evaluated their RXR agonist activity, and performed structure−activity relationship analysis. Reporter gene assay revealed that though **6b**, which possesses an amino group at the 2-position of 5-carboxybenzimidazole, showed RXR full-agonist activity, compounds **6d** and **6e**, which possess an oxygen atom and a sulfur atom at the corresponding position, respectively, showed weak RXR agonist activity. On the other hand, **6c**, which has a trifluoromethyl group at the corresponding position, acts as an RXR partial agonist, having similar E_{max} (67 ± 2%) and lower EC_{50} (15 ± 0 nM) compared to those of **4a** (E_{max} = 75 ± 4%, EC_{50} = 143 ± 2 nM). A fluorescence polarization assay of cofactor recruitment confirmed that fluorescein-labeled D22 coactivator peptide was less efficiently recruited to RXR by **4a** and **6c** than by LGD1069 (**1**), a known RXR full agonist. Electrostatic potential field calculations and computational docking studies suggested that full agonists show an electrostatic attraction, which stabilizes the holo structure and favors coactivator recruitment, between the side chain at the benzimidazole 2-position and the α-carbonyl oxygen of asparagine-306 in helix 4 (H4) of the RXR receptor. However, RXR partial agonists **4a** and **6c** lack this interaction. Like **4a**, **6c** showed a significant antidiabetes effect in KK-A^y type 2 diabetes model mice with reduced levels of the side effects associated with RXR full agonists. These findings should aid the design of new RXR partial agonists as antitype 2 diabetes drug candidates.

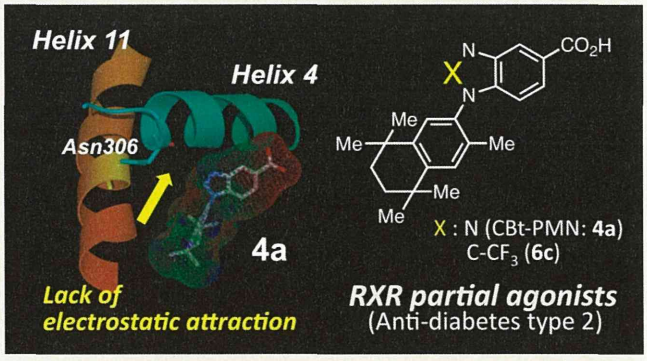

INTRODUCTION

Retinoid X receptors (RXRs) are nuclear receptors that act as ligand-dependent transcription factors and function as the homodimer or as heterodimers with other nuclear receptors, such as retinoic acid receptors (RARs), peroxisome proliferator-activated receptors (PPARs), or liver X receptors (LXRs).[1−3] Interestingly, so-called permissive heterodimers, such as PPAR/RXR[4−6] and

Received: October 3, 2012
Published: February 7, 2013

LXR/RXR,[7−10] which regulate glucose/lipid metabolism and immune response, can be activated by RXR agonists alone.[11] Therefore, RXR agonists are considered to be candidate therapeutic agents for the treatment of type 2 diabetes and autoimmune disease. In addition, synthetic RXR agonists are being used as therapies for other indications. For example, bexarotene (**1**) is approved for treatment of subcutaneous T-cell lymphoma (STCL) in the United States.[12] Although several RXR agonists have been created (Figure 1),[13−17] they were

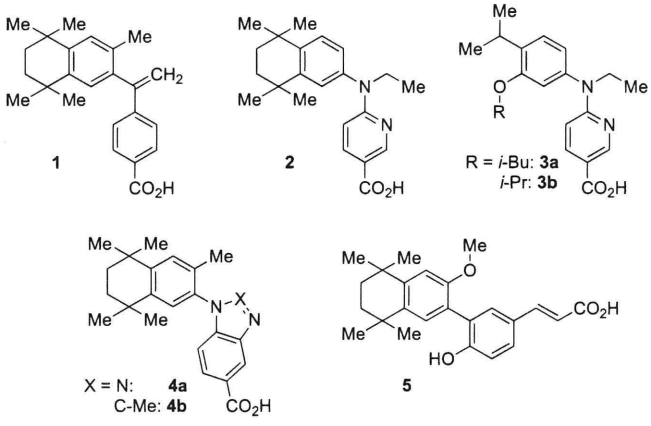

Figure 1. Chemical structures of known RXR ligands **1**−**5**.

found to induce body weight gain,[18] hepatomegaly,[19] blood triglyceride (TG) elevation,[20] and other adverse effects. However, it has been reported that RXR agonists show different patterns of RXR heterodimer activation.[21] Further, when we evaluated the therapeutic and side effects of NEt-TMN (**2**), NEt-3IB (**3a**), and NEt-3IP (**3b**) in KK-A^y type 2 diabetes model mice, we found similar activation of RXR homodimer but different patterns of RXR heterodimer activation.[22] These compounds show therapeutic effects, but also show some of the side effects reported for other RXR agonists.

All RXR agonists that exhibit severe side effects are RXR full agonists, which activate RXR completely. Thus, in our previous work, we hypothesized that there is a difference in RXR activation threshold for the appearance of the therapeutic effects and the side effects. In other words, we considered that RXR partial agonists, whose maximum activation of RXR is lower than that of RXR full agonists, might induce the desired medicinal effects without (or at least with reduced levels of) the side effects that are associated with RXR full agonists. To test this idea, we designed and synthesized RXR partial agonists based on **1** or **2** by linking the acidic domain and the linking domain of **1** or **2**, with the aim of restricting the molecular flexibility. This approach yielded the RXR partial agonist CBt-PMN (**4a**), which indeed showed a significant antidiabetes effect in KK-A^y type 2 diabetes model mice but with reduced levels of the side effects associated with RXR full agonists.[16] However, the reason why **4a** acts as an RXR partial agonist was not established.

In the present work, we aimed to elucidate the mechanism of RXR partial agonistic activity of **4a**, and for this purpose we synthesized a series of derivatives of **4a** for structure−activity relationship analysis. We noted that CBiM-PMN (**4b**),[16] which possesses a methyl group at the benzimidazole 2-position, shows RXR full agonistic activity, and thus we considered that the heterocyclic moiety, especially the 2-position, might be critical for RXR agonistic activity. Therefore, we focused on modification of the heterocyclic ring of **4a** at the 2-position (Figure 2).

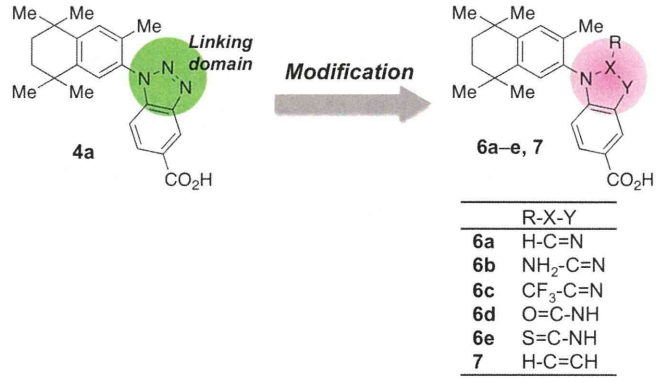

Figure 2. Molecular design strategy for creating derivatives of **4a**.

Indeed, we found that **6c**, which possesses a trifluoromethyl group at the benzimidazole 2-position, has similar E_{max} and lower EC_{50} values compared to those of **4a**, showing that **6c** is a more potent RXR partial agonist than **4a**. To interpret the structure−activity relationship findings, we carried out electrostatic potential field calculations and computational docking studies. The results indicated that docked RXR full agonists exhibit an electrostatic attraction between the side chain at the benzimidazole 2-position and the α-carbonyl oxygen of asparagine-306 in helix 4 (H4) of the RXR receptor. Such an interaction would serve to stabilize the holo structure, favoring coactivator recruitment. However, RXR partial agonists **4a** and **6c** lack this interaction. We also confirmed that **6c** shows a significant antidiabetes effect in KK-A^y type 2 diabetes model mice with reduced levels of the side effects associated with RXR full agonists.

CHEMISTRY

Compounds were synthesized as illustrated in Schemes 1 and 2. Compound **10** was synthesized by nitration and hydrogen reduction from **8**, the synthesis of which has already been reported.[16] On the other hand, compound **13** was obtained from 4-iodobenzoic acid (**11**) by nitration and protection of the carboxyl group as the methyl ester. Compound **14** was synthesized from **10** and **13** by Buchwald coupling reaction, and the common intermediate **15** was obtained from **14** by hydrogen reduction. Compounds **16a**−**e** were synthesized by a ring-closing reaction using formic acid, cyanogen bromide, trifluoroacetic anhydride, triphosgene, and carbon disulfide, respectively. Hydrolysis of the ester group under alkaline conditions afforded the desired products **6a**−**e** (Scheme 1). Compound **7** was obtained by alkaline saponification from **19**, which was synthesized from **17** (obtained as previously reported[23]) and **18** by Ullmann condensation (Scheme 2).

RESULTS AND DISCUSSION

The compounds obtained were evaluated by reporter gene assay using COS-1 cells (Table 1). Among the compounds bearing a side chain at the 2-position in the benzimidazole ring, amino derivative **6b** activated RXRα as potently as **2** and **4b**, as previously reported.[16] Compounds **6d** and **6e** showed low efficacy, even at 10 μM. On the other hand, compound **6a**, which has no side chain at the 2-position in the benzimidazole ring, as well as trifluoromethyl derivative **6c** and compound **7**

dx.doi.org/10.1021/jm400033f | J. Med. Chem. 2013, 56, 1865−1877

Scheme 1[a]

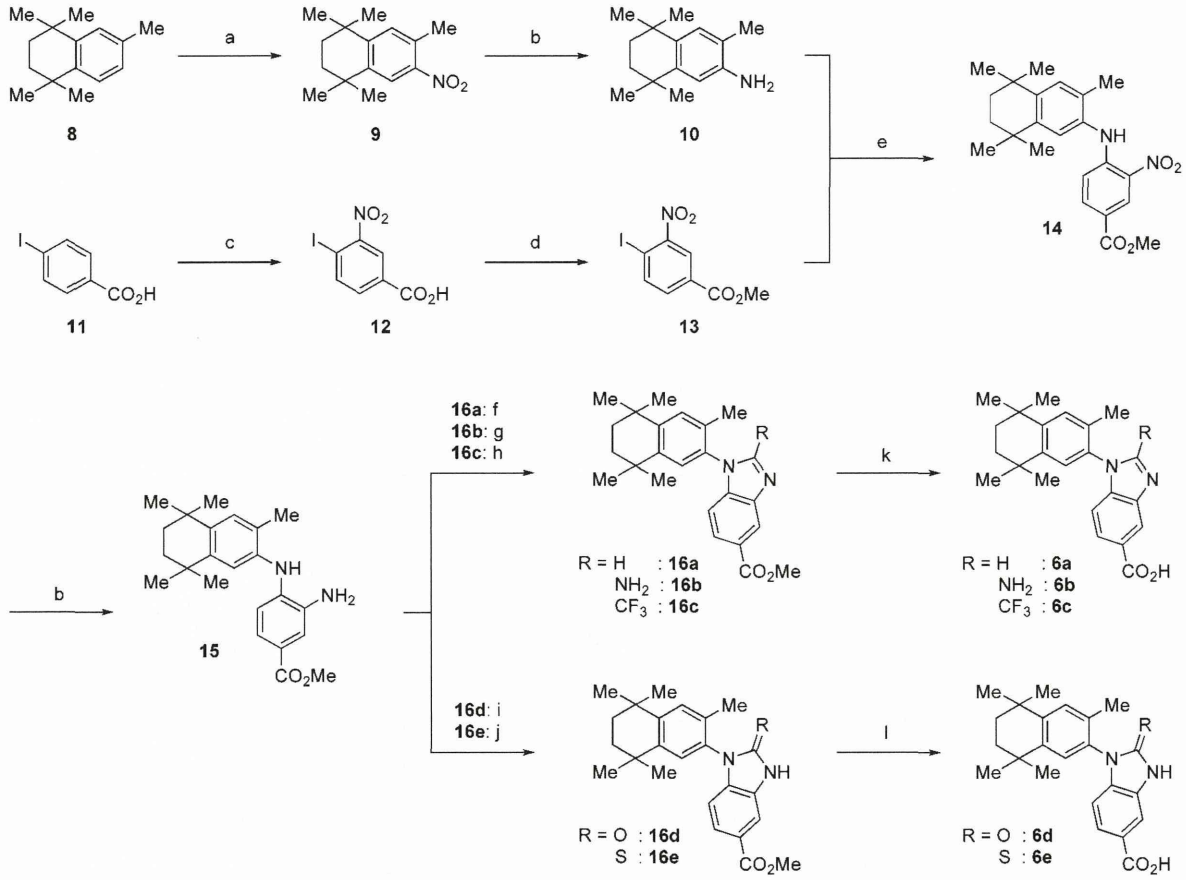

[a](a) HNO_3, Ac_2O, 72%. (b) H_2, Pd–C, EtOAc, 84%–qy. (c) HNO_3, H_2SO_4, 90%. (d) H_2SO_4, MeOH, qy. (e) $Pd_2(dba)_3$, *rac*-BINAP, Cs_2CO_3, toluene, qy. (f) HCO_2H, 93%. (g) BrCN, THF, 26%. (h) TFAA, TFA, 95%. (i) Triphosgene, TEA, DCE, qy. (j) CS_2, DBU, DMF, 93%. (k) (1) 2 N NaOH, MeOH, THF; (2) 2 N HCl, 43%–qy. (1) 2 N NaOH, MeOH; (2) 2 N HCl, 86%–qy.

Scheme 2[a]

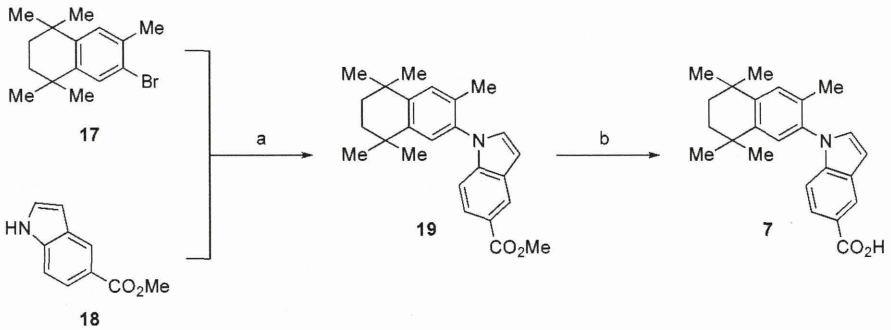

[a](a) CuI, DMEDA, K_3PO_4, toluene, 7.9%. (b) (1) 2 N NaOH, MeOH, THF; (2) 2 N HCl, 92%.

possessing an indole structure, showed lower E_{max} values than those of **2**, **4b**, and **6b**.

According to the review by Pierre Germain et al., nuclear receptor partial agonists are defined as ligands that are potent but exhibit reduced efficacy when compared with full agonists.[24] These compounds can also induce antagonist conformation. For example, PPARγ partial agonist GW0072 is reported to act as a competitive antagonist of rosiglitazone, a PPAR full agonist, despite exhibiting weak PPARγ agonist activity.[25] Thus, to examine whether **6a**, **6c**, and **7** are RXR partial agonists, we evaluated their competitive antagonistic activity against 1 μM **1**. The dose–response curves in the absence of **1** showed that **4a**, **6a**, **6c**, and **7** exhibit RXR agonist activity (Figure 3a). However, since only **4a** and **6c** behaved as competitive antagonists in the presence of **1** (Figure 3b), only these two compounds were considered to be RXR partial agonists.

The ligand-dependent transcription of RXR dimers is induced by conformational change of the receptor from the apo-form (a ligand-free form that recruits a corepressor) to the holo-form (an agonist-binding form that recruits a coactivator).[26] RXR partial agonists are thought to recruit both coactivators and corepressors, acting also as RXR partial antagonists, and it is thought that the recruitment of each type of cofactor by partial agonists is less efficient than that by full

dx.doi.org/10.1021/jm400033f | J. Med. Chem. 2013, 56, 1865–1877

Table 1. Cotransfection Data for 2, 4a, 4b, 6a–e, and 7 towards RXRα in COS-1 Cells and Substituent Constants at the Heterocyclic 2-Position

	efficacy[a,b] (%)					properties of R	
compd	at 0.1 μM	at 1 μM	at 10 μM	EC_{50} (nM)[c]	E_{max} (%)	Es[d]	π[e]
2	86 ± 2	96 ± 4	98 ± 3	3.8 ± 0.2	96 ± 4	–	–
4a	24 ± 2	75 ± 3	69 ± 3	143 ± 2	75 ± 4	–	–
4b	28 ± 1	70 ± 4	80 ± 5	367 ± 130	94 ± 5	−1.24	0.56
6a	NA	52 ± 3	72 ± 4	633 ± 33	75 ± 3	0.00	0.00
6b	NA	35 ± 3	96 ± 4	155 ± 10	103 ± 2	−0.61	−1.23
6c	21 ± 2	65 ± 1	71 ± 6	15 ± 0	67 ± 2	−2.40	0.88
6d	NA	NA	22 ± 2	–	–	–	–
6e	NA	NA	37 ± 0	–	–	–	–
7	45 ± 3	67 ± 5	77 ± 4	83 ± 8	73 ± 2	0.00	0.00

[a]The relative transactivation activity is based on the luciferase activity of 1 μM **1** (RXR full agonist) taken as 100%. All values represent the mean value of at least three separate experiments with triplicate determinations. [b]NA means nonactive (the value is less than 5). [c]EC_{50} values were determined from full dose–response curves. [d]Es: Taft's steric substituent constant (steric effect). [e]π: lipophilicity. These data were cited from Hansch, C.; Leo, A. *Substituent Constants for Correlation Analysis in Chemistry and Biology*; Wiley-Interscience: New York, 1979.

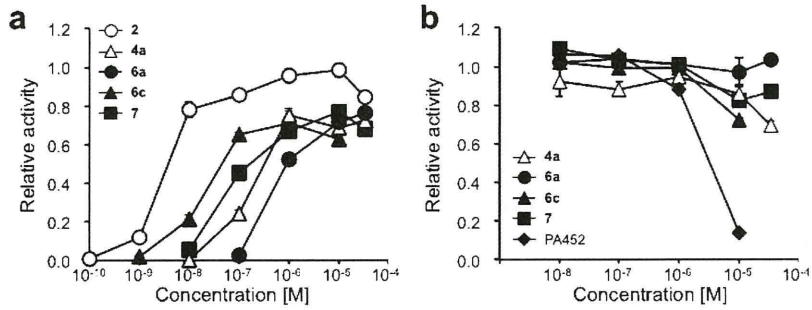

Figure 3. Relative transactivation activities of **2**, **4a**, **6a**, **6c**, and **7** toward RXRα. (a) Dose-dependence of RXRα agonist activities of **2** (open circles), **4a** (open triangles), **6a** (closed circles), **6c** (closed triangles), and **7** (closed squares). (b) Dose-dependence of RXRα antagonist activities of **4a** (open triangles), **6a** (closed circles), **6c** (closed triangles), **7** (closed squares), and PA452 (closed diamond) in the presence of 1 μM **1**. The transactivation activity is shown as relative activity based on the luciferase activity of 1 μM **1** taken as 1.0. Error bars are SEM.

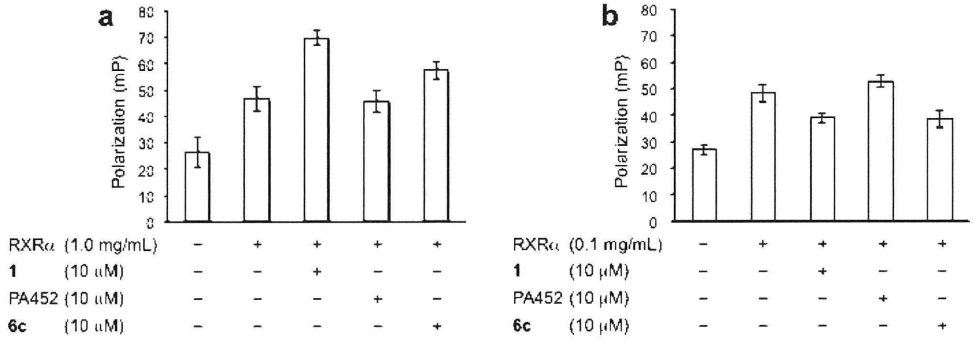

Figure 4. Changes in fluorescence polarization of (a) 5 nM fluorescein-labeled coactivator peptide D22 or (b) 5 nM fluorescein-labeled corepressor peptide SMRT-ID2 induced by **6c** (putative partial agonist), compound **1** (RXR full agonist), and PA452 (RXR antagonist). Fluorescence polarization values, expressed in mP, are the mean ± SEM of measurements obtained from triplicate wells.

agonists or full antagonists. Thus, we examined cofactor recruitment by our putative RXR partial agonists. Cofactor recruitment assay was performed using fluorescence polarization measurements with RXR receptor, each ligand and fluorescein-labeled cofactors according to Lévy-Bimbot et al.[27,28] If a fluorescein-labeled cofactor does not bind to the receptor, the degree of fluorescence polarization (FP) will be low, because the fluorescein-labeled cofactor retains high mobility. However, binding of the cofactor to the receptor reduces the mobility and induces a high FP value. Thus, addition of an agonist to a mixture of fluorescein-labeled coactivator and RXR receptor should result in a higher FP value than that in its absence.

As coactivator and corepressor peptides, we selected D22[29] and silencing mediator for retinoid and thyroid hormone receptors interaction domain 2 (SMRT-ID2),[30] respectively. D22 has been used for time-resolved fluorescence resonance energy transfer (TR-FRET) assay with RXR.[29] SMRT-ID2 is reported to bind to apo-RXR.[30] First, to determine the appropriate RXR concentration for this assay, we evaluated FP values at various RXR concentrations with each fluorescein-labeled cofactor (5 nM) in the absence or presence of **1** (1 μM). As the

dx.doi.org/10.1021/jm400033f | J. Med. Chem. 2013, 56, 1865–1877

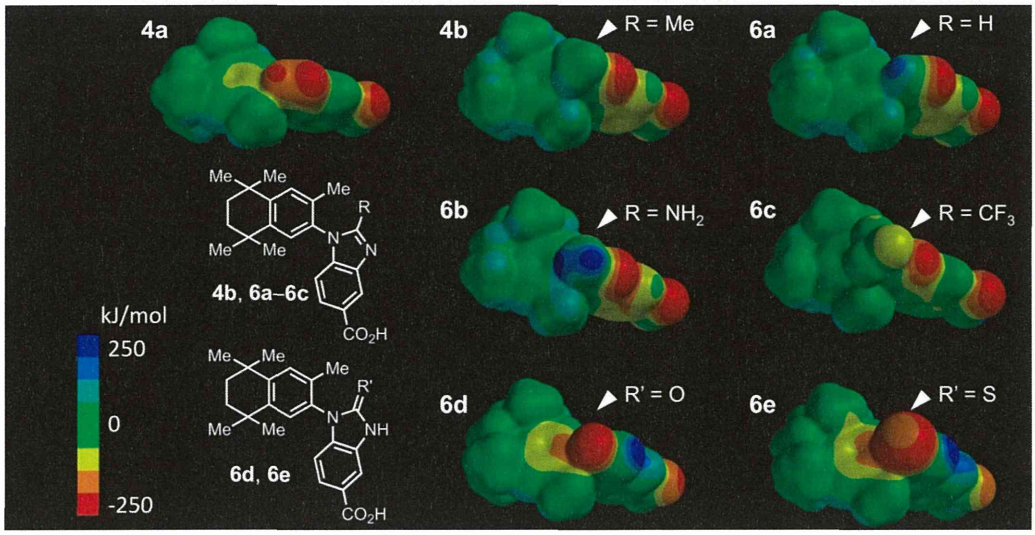

Figure 5. Calculated electrostatic potential distribution of **4a**, **4b**, and **6a–e**.

RXR concentration was increased, the FP value also increased, indicating the binding of each peptide with RXR (Supporting Information, Figure S1). In the presence of full agonist **1**, the plot for fluorescein-labeled D22 was shifted to the left, indicating that **1** induced interaction of D22 with RXR. On the other hand, the plot for fluorescein-labeled SMRT-ID2 was shifted to the right in the presence of **1**, indicating that **1** decreased the interaction between SMRT-ID2 and RXR. The RXR concentration showing the largest change of FP by **1** was 1.0 mg/mL for fluorescein-labeled D22 or 0.1 mg/mL for SMRT-ID2, and therefore these RXR concentrations were used in subsequent experiments. Using these conditions, we compared the cofactor recruitment ability of RXR partial agonists **4a** and **6c** with those of RXR full agonist **1** and RXR antagonist PA452.[31] Each compound was used at 10 μM, because we found no difference in recruitment of fluorescein-labeled D22 between 10 and 33 μM concentrations (Supporting Information, Figure S2). As shown in Figures S2 (Supporting Information) and 4, the coactivator recruitment ability of both RXR partial agonists was intermediate between those of RXR full agonist **1** and RXR antagonist PA452. On the other hand, the corepressor recruitment ability of RXR partial agonist **6c** was less than that of PA452 and similar to that of RXR full agonist **1**. Taken together with the results of reporter gene assay and cofactor recruitment assay, these findings confirm that **6c** is a RXR partial agonist, like **4a**.

To examine the effects of substituents at the benzimidazole 2-position, we performed structure–activity relationship analysis of **2**, **4a**, **4b**, and **6a–c** (Table 1). Considering their Taft's steric substituent constants (Es) and lipophilicity (π), we found that these two constants appeared not to be related to RXR agonistic activity, indicating that electronic properties at the benzimidazole 2-position are critical for RXR agonistic activity.

Thus, to investigate the spatial electronic properties of these compounds, we calculated the electrostatic potential field using Spartan 10 (Figure 5). The RXR full agonists **4b** and **6b** have a positive electrostatic potential field at the benzimidazole 2-position, while RXR partial agonist **6c** has a weak negative electrostatic potential field at that position. On the other hand, **6d** and **6e**, which showed weak RXR agonistic activity, have a stronger negative electrostatic potential field at the benzimidazole 2-position than **6c**. These results suggest that a positive electrostatic potential field at the benzimidazole 2-position, as in **4b** and **6b**, is important to stabilize the holo structure, thereby favoring coactivator recruitment for RXR full agonistic activity.

Next, to examine the interaction between the electrostatic potential field around the heterocyclic 2-position and RXRα, we performed a docking study using AutoDock 4.2[32] (Figure 6

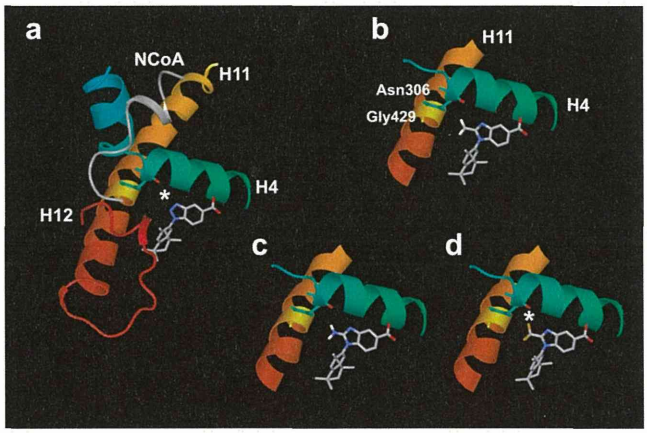

Figure 6. (a) Docking model of RXR partial agonist **4a** in the ligand-binding pocket of RXRα (PDB code 3H0A). H4, H11, and H12 mean helix 4 (jade green), helix 11 (orange), and helix 12 (red), respectively. (b) Docking model of RXR full agonist **4b** in the ligand-binding pocket of RXRα. (c) Docking model of RXR full agonist **6b** in the ligand-binding pocket of RXRα. (d) Docking model of RXR partial agonist **6c** in the ligand-binding pocket of RXRα. The asterisk indicates electrostatic repulsion.

and Table 2). The results reveal that the 2-position of the heterocyclic ring in **4a**, **4b**, **6b**, and **6c** is close to the α-carbonyl oxygen of asparagine-306 (Asn306) in helix 4 (H4; jade green). Thus, full agonists **4b** and **6b**, which have a positive electrostatic potential field at the 2-position of the heterocyclic ring, may have an attractive interaction with Asn306 in H4. In turn, this interaction may promote the proper folding of helix 12 (H12; red), stabilizing the holo form and thus favoring recruitment of a coactivator. On the other hand, **6d** and **6e**, which have a strong negative electrostatic potential field at the

dx.doi.org/10.1021/jm400033f | J. Med. Chem. 2013, 56, 1865–1877

Table 2. Docking Score and Distance between the α-Carbonyl Oxygen of Asn306 and the Closest Atom at the Heterocyclic 2-Position of Each Compound

compd	docking score	mean binding energy (kcal/mol)	distance (Å)	atom
2	–	–	–	–
4a	100/100	−11.92	4.42	N
4b	100/100	−12.13	2.67	H
6a	100/100	−11.45	3.85	H
6b	100/100	−11.72	2.66	H
6c	100/100	−11.41	2.51	F
6d	100/100	−11.49	3.88	O
6e	100/100	−11.97	3.39	S
7	100/100	−11.67	3.88	H

2-position of the heterocyclic ring, would exhibit electrostatic repulsion between the 2-position of the heterocyclic ring and Asn306. Such electrostatic repulsion may reduce the affinity for RXR and lead to a steric clash between Asn306 in H4 and glycine-429 (Gly429) in helix 11 (H11; orange), thereby unstabilizing the holo form. On the other hand, compounds **4a** and **6c** lack the electrostatic attractive force because these compounds possess a weak negative electrostatic field around the 2-position of the heterocyclic ring. Thus, RXR partial agonists might be less able to induce stable folding of H12 in RXR for coactivator recruitment, as compared to RXR full agonists. These results suggest that the nature of the interaction between a ligand and H4 is important for determining whether the ligand exerts RXR full agonistic or partial agonistic activity.

We found that **6c** is a more potent RXR partial agonist than **4a**. Thus, we next examined the activities of **6c** toward other RXR subtypes, as well as RARs, PPARγ, LXRα, PPARγ/RXRα, and LXRα/RXRα, by means of reporter gene assay. Compound **6c** showed partial agonistic activities toward RXRβ and RXRγ, but caused little activation of RARs (Supporting Information, Figure S3). In addition, **6c** showed no PPARγ agonistic activity but activated LXRα, LXRα/RXRα, and PPARγ/RXRα (Supporting Information, Figure S4). Compounds **4a** and **6c** also showed RXR partial agonist activity toward mouse RXRα (Supporting Information, Figure S5), as well as human RXRα. Thus, **6c** can be expected to show antidiabetic effects in mice, similar to **4a**.

Since **6c** shows similar receptor activation patterns to **4a**,[16] we were interested in the anti-type 2 diabetes effect and the side effects of **6c**. First, we confirmed that single oral administration of **6c** at 30 mg/kg resulted in a blood concentration over 6 μM in ICR male mice (Supporting Information, Figure S6). Then, to evaluate side effects associated with RXR full agonists, changes in body weight, hepatomegaly, blood triglyceride (TG), and blood total cholesterol (TCHO) were assessed when **6c**, RXR full agonist **2**, and **4b** were administered orally to ICR mice at 30 mg/kg/day for 7 days (Figure 7). Despite developing slight hepatomegaly, the group treated with **6c** showed a similar body weight gain to the control group and did not show blood TG or TCHO elevation, whereas the group treated with **2** or **4b** showed significant increases of body weight gain and blood TG level compared with the control. We found no significant differences of renal function parameters between the treated and the vehicle control groups (Supporting Information, Table S2). Since liver function parameters (in particular, alkaline phosphatase, ALP) were elevated, the hepatomegaly may be associated with hepatotoxicity related to the chemical

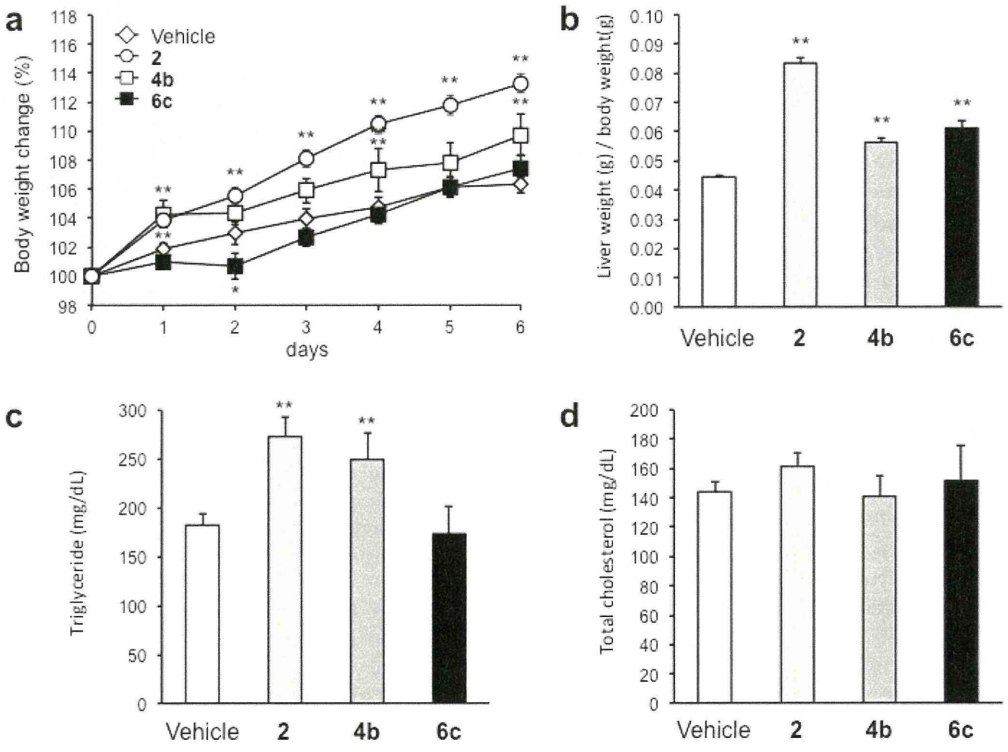

Figure 7. Evaluation of adverse effects of repeated oral administration of compounds at 30 mg/kg/day to male ICR mice for 7 consecutive days. (a) Time course of body weight change. Diamond, circles, open squares, and closed squares indicate vehicle, **2**, **4b**, and **6c**, respectively. Effects of compounds on (b) liver weight gain, (c) serum triglyceride, and (d) total cholesterol, respectively. The data (n = 7–23) represent the mean ± SEM. Statistical analysis was performed by analysis of variance (ANOVA). Significant difference: *p < 0.05 vs vehicle. **p < 0.01 vs vehicle.

dx.doi.org/10.1021/jm400033f | J. Med. Chem. 2013, 56, 1865–1877

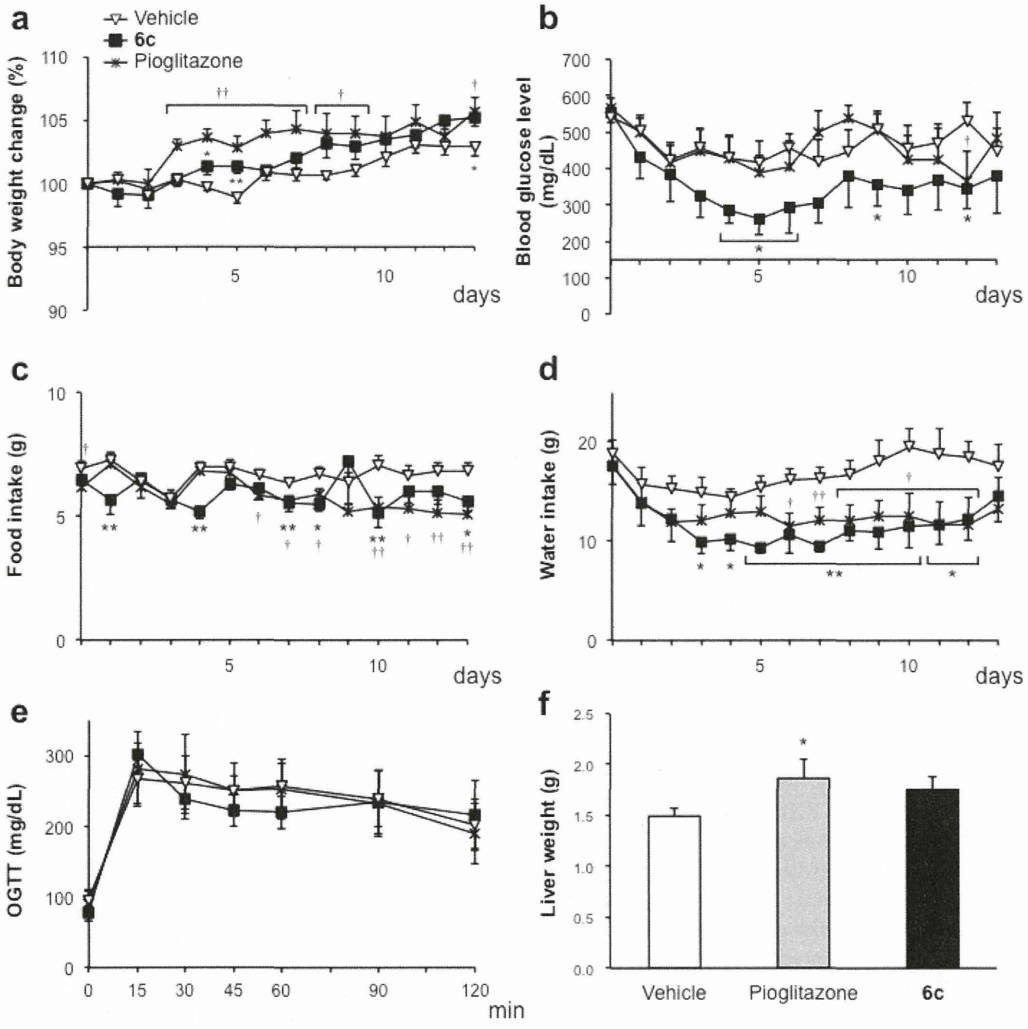

Figure 8. Evaluation of anti-type 2 diabetes effects of repeated oral administration of **6c** or pioglitazone at 10 mg/kg/day to male KK-A^y mice for 14 consecutive days. Time course of (a) body weight change, (b) blood glucose levels. (c) food intake, (d) water intake, and (e) oral glucose tolerance test (OGTT) results. (f) Liver weight gain in male KK-A^y mice treated with vehicle and compounds. Inverted triangles, closed squares, and asterisks indicate vehicle, **6c**, and pioglitazone, respectively. The data (n = 4–5) represent the mean ± SEM. Statistical analysis was performed by analysis of variance (ANOVA). Significant difference: *p < 0.05, **6c** vs vehicle. **p < 0.01, **6c** vs vehicle. †p < 0.05, pioglitazone vs vehicle. ††p < 0.01, pioglitazone vs vehicle.

structure of **6c**. Nevertheless, the hepatomegaly induced by **6c** is clearly less marked than that induced by RXR full agonist **2**.

Further, when **6c** was administered orally to male and female SD rats at 30 mg/kg/day for 28 days, we observed hepatotoxicity similar to that in the case of administration to ICR mice for 7 days, together with slight enlargement of the spleen, but there was no significant difference in body weight change or in the weights of other organs (Supporting Information, Figure S7 and Tables S3 and S4). As for blood constituents, some significant differences from the vehicle were observed, but the data, other than liver function parameters, were all within the ranges considered normal by the suppliers.

Next, we examined the antitype 2 diabetes activity in KK-A^y mice. Compound **6c** or pioglitazone was orally administered at 10 mg/kg/day for 14 days (Figure 8). The group treated with **6c** did not show significant improvement in the oral glucose tolerance test (OGTT) compared to the control group (Figure 8e), but the average blood glucose level in the group treated with **6c** was significantly reduced at days 4–6, 9, and 12 (Figure 8b). Compound **6c** also reduced water intake significantly at days 3–12 compared to vehicle-treated mice (Figure 8d), thus showing significant anti-type 2 diabetes effects.

Table 3. Plasma Parameters of Male KK-A^y Mice after Oral Administration of Vehicle, 6c, or Pioglitazone at 10 mg/kg/day for 14 Consecutive Days[a]

	vehicle	pioglitazone	6c
AST (U/I)	49.6 ± 2.3	45.3 ± 8.4	42.3 ± 2.9
ALT (U/I)	17.6 ± 0.9	21.3 ± 1.9*	17.3 ± 2.6
γ-GTP (U/I)	5.8 ± 0.6	7.3 ± 2.3	6.3 ± 0.3
ALP (U/I)	358.2 ± 43.1	395.7 ± 44.1	554.0 ± 113.2*
CRE (mg/dL)	DL	DL	DL
BUN (mg/dL)	21.9 ± 1.1	22.2 ± 1.3	22.5 ± 1.1
TG (mg/dL)	122.4 ± 11.0	124.0 ± 28.5	185.0 ± 38.0
TCHO (mg/dL)	153.2 ± 11.1	147.3 ± 3.8	155.3 ± 10.7

[a]The data (n = 3–5) represent the mean ± SEM. Statistical analysis was performed by analysis of variance (ANOVA). Significant difference: *p < 0.05 vs vehicle. **p < 0.01 vs vehicle. DL means detection limit (0.2 mg/dL).

dx.doi.org/10.1021/jm400033f | J. Med. Chem. 2013, 56, 1865–1877

These effects also may result partially or entirely from activation of PPAR/RXR or LXR/RXR activation by **6c**. Moreover, **6c** did not elevate blood TG or blood TCHO significantly (Table 3). These results support our hypothesis of a threshold difference for the therapeutic and side effects of RXR agonists and indicate that RXR partial agonists represent a promising class of candidate anti-type 2 diabetes agents with reduced levels of the serious adverse effects caused by RXR full agonists.

CONCLUSION

In order to elucidate the mechanism of action of the RXR partial agonist **4a**, we synthesized several derivatives of **4a** and performed structure−activity relationship analysis. The results of electrostatic potential field calculations and computational docking studies indicated that the electrostatic attraction between an oxygen atom of Asn306 in H4 and the 2-position at the benzimidazole ring, which is observed in RXR full agonists, is absent in the partial agonists **4a** (reported previously) and **6c** (newly synthesized in this work). The presence of this interaction would stabilize the holo form of RXR and favor coactivator recruitment. Compound **6c** showed similar E_{max} and lower EC_{50} values toward RXR compared to **4a**. Fluorescence polarization assay of cofactor recruitment confirmed its partial agonist character. We evaluated its side effects in ICR mice and SD rats, as well as its therapeutic effects in the KK-A^y mouse model of type 2 diabetes. Although **6c** induced slight hepatomegaly, the degree of hepatomegaly was less than that induced by RXR full agonists **2** and **4b**. We confirmed that **6c** had a significant antidiabetes effect in KK-A^y type 2 diabetes model mice with less side effects than RXR full agonists. These results indicate that RXR partial agonists are promising candidates for antidiabetes drugs with reduced levels of the side effects associated with full agonists. Further structural modification of our compounds may generate attractive candidates for antitype 2 diabetes agents.

EXPERIMENTAL SECTION

Chemistry. *General.* Melting points were determined with a Yanagimoto hot-stage melting point apparatus and are uncorrected. IR spectra were recorded on a JASCO FT/IR350 (KBr). ^{1}H NMR spectra were recorded on a JEOL JNM-AL300 FT-NMR system (300 MHz), a Varian VXR-300 (300 MHz) spectrometer, or a Varian VXR-500 (500 MHz) spectrometer. FAB-MS was carried out with a VG70-SE. The purity of all tested compounds was >95%, as confirmed by combustion analysis or by HPLC analysis. Elemental analysis was carried out with a Yanagimoto MT-5 CHN recorder elemental analyzer, and results were within ±0.4% of the theoretical values. The HPLC system used in this study was a Shimadzu liquid chromatographic system (Kyoto, Japan) consisting of an LC-10AD pump, SPD-10AV UV−vis spectrophotometric detector, CTO-10AS column oven and C-R5A Chromatopac. The samples (each 20 μL) were injected and the chromatographic analyses were carried out on an Inertsil ODS-3 (4.6 i.d. × 250 mm, 5 μm, GL Sciences, Tokyo, Japan) with a guard column of Inertsil ODS-3 (4.0 i.d. × 10 mm, 5 μm, GL Sciences) at 40 °C, using methanol:16.7−50 mM ammonium acetate (final concentration at 5 mM) (adjusted with acetic acid to pH 5.0) (90:10, 80:20, or 70:30, v/v) as a mobile phase. The flow rate was 0.7 mL/min and the absorbance at 280 nm was monitored.

*4-[1-(3,5,5,8,8-Pentamethyl-5,6,7,8-tetrahydronaphthalen-2-yl)-ethenyl]benzoic Acid (**1**).* This compound was prepared according to ref 13. HPLC: 11.6 min; >95% purity (MeOH:$AcONH_4$(aq) = 90:10).

*6-[Ethyl(5,5,8,8-tetramethyl-5,6,7,8-tetrahydronaphthalen-2-yl)-amino]nicotinic Acid (**2**).* This compound was prepared according to ref 14. HPLC: 24.9 min; >95% purity (MeOH:$AcONH_4$(aq) = 80:20).

*1-(3,5,5,8,8-Pentamethyl-5,6,7,8-tetrahydro-2-naphthyl)-1H-benzotriazole-5-carboxylic Acid (**4a**).* This compound was prepared according to ref 16. HPLC: 13.8 min; >95% purity (MeOH:$AcONH_4$(aq) = 80:20).

*2-Methyl-1-(3,5,5,8,8-pentamethyl-5,6,7,8-tetrahydro-2-naphthyl)-1H-benzoimidazole-5-carboxylic Acid (**4b**).* This compound was prepared according to ref 16. HPLC: 14.0 min; >95% purity (MeOH:$AcONH_4$(aq) = 80:20).

*1,1,4,4,6-Pentamethyl-7-nitro-1,2,3,4-tetrahydronaphthalene (**9**).* To an ice-cooled solution of **8** (2.0 g, 9.9 mmol) in Ac_2O (10 mL) was added dropwise concd HNO_3 (0.75 mL). The reaction mixture was poured into ice and extracted with EtOAc (2 × 50 mL). The organic layer was washed with H_2O (2 × 50 mL) and brine (50 mL), dried over $MgSO_4$, and evaporated under reduced pressure. The residue was recrystallized from EtOAc/hexane to yield 4.5 g of **9** as a pale yellow powder (72%). ^{1}H NMR (300 MHz, $CDCl_3$) δ: 7.96 (s, 1H), 7.21 (s, 1H), 2.56 (s, 3H), 1.70 (s, 4H), 1.30 (s, 6H), 1.29 (s, 6H).

*3,5,5,8,8-Pentamethyl-5,6,7,8-tetrahydronaphthalen-2-ylamine (**10**).* To a solution of **9** (2.5 g, 10 mmol) in EtOAc (20 mL) was added Pd/C (catalytic amount). The mixture was stirred at room temperature (rt) under a H_2 atmosphere for 7.0 h, filtered through Celite, and evaporated under reduced pressure to yield 2.2 g of **10** as a pale yellow solid (qy). ^{1}H NMR (300 MHz, $CDCl_3$) δ: 6.97 (s, 1H), 6.61 (s, 1H), 3.45 (br s, 2H), 2.14 (s, 3H), 1.64 (s, 4H), 1.24 (s, 6H), 1.24 (s, 6H).

*4-Iodo-3-nitrobenzoic Acid (**12**).* To a solution of **11** (2.5 g, 10 mmol) in concd H_2SO_4 (14 mL) was added dropwise a solution of concd HNO_3 (4.9 mL) and concd H_2SO_4 (4.3 mL). The reaction mixture was stirred at rt overnight, poured onto ice (50 mL), and filtered. The filtrate was evaporated, and the residue was dried to yield 2.6 g of **12** as a pale yellow powder (90%). ^{1}H NMR (500 MHz, $CDCl_3$) δ: 8.49 (s, 1H), 8.19 (d, J = 8.0 Hz, 1H), 7.92 (d, J = 8.0 Hz, 2H).

*4-Iodo-3-nitrobenzoic Acid Methyl Ester (**13**).* To a solution of **12** (2.6 g, 9.0 mmol) in dry MeOH (10 mL) was added dropwise concd H_2SO_4 (1.9 mL). The reaction mixture was stirred at rt overnight, neutralized with sat. $NaHCO_3$ (10 mL), and extracted with EtOAc (3 × 40 mL). The organic layer was washed with H_2O (40 mL) and brine (50 mL), dried over $MgSO_4$, and evaporated under reduced pressure. The residue was recrystallized from MeOH to yield 2.8 g of **13** as yellow needles (qy). ^{1}H NMR (500 MHz, $CDCl_3$) δ: 8.45 (d, J = 2.0 Hz, 1H), 8.15 (d, J = 8.0 Hz, 1H), 7.88 (dd, J = 8.0, 2.0 Hz, 1H), 3.97 (s, 3H).

*3-Nitro-4-(3,5,5,8,8-pentamethyl-5,6,7,8-tetrahydronaphthalen-2-ylamino)benzoic Acid Methyl Ester (**14**).* To a solution of **10** (0.83 g, 3.8 mmol) and **13** (1.2 g, 3.8 mmol) in dry toluene (4.0 mL) were added $Pd_2(dba)_3$ (170 mg, 0.19 mmol), *rac*-BINAP (180 mg, 0.28 mmol), and Cs_2CO_3 (3.1 g, 9.5 mmol). The reaction mixture was refluxed at 110 °C under an Ar atmosphere overnight and filtered through Celite. The filtrate was evaporated under reduced pressure. The residue was purified by flash column chromatography (EtOAc:*n*-hexane = 1:15) to yield 1.3 g of **14** as a yellow foam (qy). ^{1}H NMR (300 MHz, $CDCl_3$) δ: 9.63 (br s, 1H), 8.93 (d, J = 2.0 Hz, 1H), 7.93 (dd, J = 9.0, 2.0 Hz, 1H), 7.24 (s, 1H), 7.17 (s, 1H), 6.82 (d, J = 9.0 Hz, 1H), 3.91 (s, 3H), 2.19 (s, 3H), 1.70 (s, 4H), 1.31 (s, 6H), 1.25 (s, 6H).

*3-Amino-4-(3,5,5,8,8-pentamethyl-5,6,7,8-tetrahydronaphthalen-2-ylamino)benzoic Acid Methyl Ester (**15**).* To a solution of **14** (0.50 g, 1.3 mmol) in EtOAc (2.0 mL) was added Pd/C (catalytic amount). The mixture was stirred at rt under a H_2 atmosphere overnight and then filtered through Celite. The filtrate was evaporated under reduced pressure to yield 0.39 g of **15** as a white solid (84%). ^{1}H NMR (300 MHz, $CDCl_3$) δ: 7.49 (s, 1H), 7.48 (d, J = 8.0 Hz, 1H), 7.13 (s, 1H), 6.96 (s, 1H), 6.83 (d, J = 8.0 Hz, 1H), 5.39 (br s, 1H), 3.87 (s, 3H), 3.55 (br s, 2H), 2.19 (s, 3H), 1.67 (s, 4H), 1.28 (s, 6H), 1.21 (s, 6H).

*1-(3,5,5,8,8-Pentamethyl-5,6,7,8-tetrahydronaphthalen-2-yl)-1H-benzoimidazole-5-carboxylic Acid Methyl Ester (**16a**).* To compound **15** (150 mg, 0.40 mmol) was added formic acid (1.0 mL). The reaction mixture was refluxed at 100 °C for 4.0 h, poured into 2 N NaOH (10 mL), and extracted with EtOAc (3 × 40 mL). The organic layer was collected, washed with brine (10 mL), and dried over $MgSO_4$. The solvent was evaporated under reduced pressure.

The residue was purified by flash column chromatography (EtOAc:*n*-hexane = 1:4) to yield 140 mg of **16a** as a colorless powder (93%). ^{1}H NMR (300 MHz, $CDCl_3$) δ: 8.61 (d, J = 2.0 Hz, 1H), 8.06 (s, 1H), 8.03 (dd, J = 9.0, 2.0 Hz, 1H), 7.33 (s, 1H), 7.22 (s, 1H), 7.21 (d, J = 9.0 Hz, 1H), 3.98 (s, 3H), 2.05 (s, 3H), 1.75 (s, 4H), 1.36 (s, 6H), 1.29 (s, 6H).

*2-Amino-1-(3,5,5,8,8-pentamethyl-5,6,7,8-tetrahydronaphthalen-2-yl)-1H-benzoimidazole-5-carboxylic Acid Methyl Ester (**16b**).* To a solution of BrCN (48 mg, 0.45 mmol) in THF (5.0 mL) was added **15** (110 mg, 0.30 mmol). The reaction mixture was stirred at rt under an Ar atmosphere for 12 h, poured into 2 N NaOH (10 mL), and extracted with EtOAc (3 × 60 mL). The organic layer was washed with brine (20 mL) and H_2O (40 mL), dried over $MgSO_4$, and evaporated under reduced pressure. The residue was purified by flash column chromatography (CH_2Cl_2:MeOH = 50:1) to yield 30 mg of **16b** as a white powder (26%). ^{1}H NMR (300 MHz, $CDCl_3$) δ: 8.14 (d, J = 1.5 Hz, 1H), 7.77 (dd, J = 8.5, 1.5 Hz, 1H), 7.34 (s, 1H), 7.23 (s, 1H), 6.81 (d, J = 8.5 Hz, 1H), 3.92 (s, 3H), 2.03 (s, 3H), 1.74 (s, 4H), 1.36 (s, 3H), 1.34 (s, 3H), 1.28 (s, 3H), 1.27 (s, 3H).

*1-(3,5,5,8,8-Pentamethyl-5,6,7,8-tetrahydronaphthalen-2-yl)-2-trifluoromethyl-1H-benzoimidazole-5-carboxylic Acid Methyl Ester (**16c**).* To a solution of **15** (520 mg, 1.4 mmol) in TFA (8.0 mL) was added trifluoroacetic anhydride (1.0 mL, 7.0 mmol). The reaction mixture was stirred at rt for 1.0 h, poured into sat. $NaHCO_3$ (30 mL), and extracted with EtOAc (3 × 50 mL). The organic layer was washed with H_2O (50 mL) and brine (10 mL), dried over $MgSO_4$, and evaporated under reduced pressure. The residue was purified by flash column chromatography (EtOAc:*n*-hexane = 1:20) to yield 590 mg of **16c** as a white solid (95%). ^{1}H NMR (300 MHz, $CDCl_3$) δ: 8.68 (d, J = 1.5 Hz, 1H), 8.10 (dd, J = 9.0, 1.5 Hz, 1H), 7.28 (d, J = 8.5 Hz, 1H), 7.20 (s, 1H), 7.12 (dd, J = 9.0, 0.5 Hz, 1H), 3.97 (s, 3H), 1.89 (s, 3H), 1.73 (s, 4H), 1.35 (s, 6H), 1.25 (s, 6H).

*2-Oxo-1-(3,5,5,8,8-pentamethyl-5,6,7,8-tetrahydro-2-naphthyl)-2,3-dihydro-1H-benzoimidazole-5-carboxylic Acid Methyl Ester (**16d**).* To a solution of **15** (110 mg, 0.30 mmol) in 1,2-dichloroethane (6.0 mL) were added Et_3N (70 μL, 0.50 mmol) and triphosgene (59 mg, 0.20 mmol). The mixture was refluxed at 110 °C overnight, poured into H_2O (40 mL), and extracted with EtOAc (2 × 30 mL). The organic layer was washed with H_2O (60 mL), dried over $MgSO_4$, and evaporated under reduced pressure to yield 120 mg of **16d** as a pale yellow solid (qy). ^{1}H NMR (500 MHz, $CDCl_3$) δ: 11.35 (s, 1H), 7.67 (dd, J = 8.0, 1.5 Hz, 1H), 7.60 (d, J = 1.5 Hz, 1H), 7.39 (s, 1H), 7.27 (s, 1H), 6.66 (d, J = 8.0 Hz, 1H), 3.84 (s, 3H), 2.00 (s, 3H), 1.68 (s, 4H), 1.31 (s, 3H), 1.30 (s, 3H), 1.23 (s, 3H), 1.23 (s, 3H).

*1-(3,5,5,8,8-Pentamethyl-5,6,7,8-tetrahydro-2-naphthyl)-2-thioxo-2,3-dihydro-1H-benzoimidazole-5-carboxylic Acid Methyl Ester (**16e**).* To a solution of **15** (62 mg, 0.17 mmol) in DMF (2.0 mL) were added CS_2 (100 μL, 1.7 mmol) and DBU (25 μL, 0.17 mmol). The reaction mixture was stirred at 50 °C for 0.5 h, poured into H_2O (60 mL), and extracted with EtOAc (3 × 40 mL). The organic layer was washed with H_2O (3 × 80 mL) and brine (80 mL), dried over $MgSO_4$, and evaporated under reduced pressure. The residue was purified by flash column chromatography (EtOAc:*n*-hexane = 1:5) to yield 64 mg of **16d** as a white solid (93%). ^{1}H NMR (300 MHz, $CDCl_3$) δ: 12.3 (br s, 1H), 8.00 (s, 1H), 7.89 (dd, J = 8.5, 1.5 Hz, 1H), 7.34 (s, 1H), 7.22 (s, 1H), 6.81 (d, J = 8.5 Hz, 1H), 3.92 (s, 3H), 2.08 (s, 3H), 1.74 (s, 4H), 1.36 (s, 3H), 1.35 (s, 3H), 1.31 (s, 3H), 1.26 (s, 3H).

*1-(3,5,5,8,8-Pentamethyl-5,6,7,8-tetrahydronaphthalen-2-yl)-1H-benzoimidazole-5-carboxylic Acid (**6a**).* To a solution of **16a** (140 mg, 0.40 mmol) in MeOH (3.0 mL) and THF (1.0 mL) was added 2 N NaOH (2.0 mL). The reaction mixture was stirred at 60 °C for 2.0 h, poured into 2 N HCl (2.0 mL), and extracted with EtOAc (3 × 40 mL). The organic layer was collected, washed with brine (20 mL), dried over $MgSO_4$, and evaporated under reduced pressure to yield 180 mg of **6a** (qy). The residue was recrystallized from EtOAc/*n*-hexane to yield 110 mg of colorless powder. Mp: 255.0–257.0 °C. HPLC: 13 min; 99% purity (MeOH:$AcONH_4$(aq) = 70:30). ^{1}H NMR (300 MHz, $CDCl_3$) δ: 8.76 (d, J = 2.0 Hz, 1H), 8.17 (s, 1H), 8.11 (dd, J = 8.0, 2.0 Hz, 1H), 7.33 (s, 1H), 7.27 (d, J = 8.0 Hz, 1H), 7.26 (s, 1H), 7.23 (s, 1H), 2.06 (s, 3H), 1.74 (s, 4H), 1.36 (s, 6H), 1.29 (s, 6H). FAB-MS m/z: 363 $[M + H]^+$.

*2-Amino-1-(3,5,5,8,8-pentamethyl-5,6,7,8-tetrahydronaphthalen-2-yl)-1H-benzoimidazole-5-carboxylic Acid (**6b**).* To a solution of **16b** (95 mg, 0.24 mmol) in MeOH (2.0 mL) and THF (2.0 mL) was added 2 N NaOH (2.0 mL). The reaction mixture was stirred at 60 °C for 0.5 h, poured into 2 N HCl (4.0 mL), and extracted with EtOAc (3 × 70 mL). The organic layer was collected, washed with brine (30 mL) and H_2O (30 mL), dried over $MgSO_4$, and evaporated under reduced pressure. The residue was purified by flash column chromatography (CH_2Cl_2:MeOH = 10:1) to yield 110 mg of **6b** as white crystals (qy). Mp: 226.2–227.9 °C. HPLC: 25 min; >95% purity (MeOH:$AcONH_4$(aq) = 70:30). ^{1}H NMR (300 MHz, DMSO-d_6) δ: 12.95 (br s, 1H), 8.36 (br s, 2H), 7.98 (s, 1H), 7.79 (dd, J = 8.5, 1.0 Hz, 1H), 7.53 (s, 1H), 7.50 (s, 1H), 6.79 (d, J = 8.5 Hz, 1H), 2.01 (s, 3H), 1.69 (s, 4H), 1.33 (s, 6H), 1.25 (s, 3H), 1.23 (s, 3H). FAB-MS m/z: 378 $[M + H]^+$.

*1-(3,5,5,8,8-Pentamethyl-5,6,7,8-tetrahydronaphthalen-2-yl)-2-trifluoromethyl-1H-benzoimidazole-5-carboxylic Acid (**6c**).* To a solution of **16c** (50 mg, 0.11 mmol) in MeOH (1.0 mL) and THF (2.0 mL) was added 2 N NaOH (1.0 mL). The reaction mixture was stirred at 60 °C for 1.0 h and then poured into 2 N HCl (2.0 mL) and extracted with EtOAc (3 × 40 mL). The organic layer was collected, washed with brine (10 mL) and H_2O (10 mL), dried over $MgSO_4$, and evaporated under reduced pressure. The residue was recrystallized from EtOAc/*n*-hexane to yield 21 mg of **6c** as a colorless powder (43%). Mp: 235.8–237.1 °C. ^{1}H NMR (300 MHz, $CDCl_3$) δ: 8.75 (d, J = 1.5 Hz, 1H), 8.15 (dd, J = 8.5, 1.5 Hz, 1H), 7.30 (s, 1H), 7.21 (s, 1H), 7.15 (d, J = 9.5 Hz, 1H), 1.91 (s, 3H), 1.74 (s, 4H), 1.36 (s, 6H), 1.25 (s, 6H). FAB-MS m/z: 431 $[M + H]^+$. Anal. Calcd for $C_{24}H_{25}F_3N_2O_2$: C, 66.96; H, 5.85; N, 6.51. Found: C, 66.93; H, 6.11; N, 6.41.

*2-Oxo-1-(3,5,5,8,8-pentamethyl-5,6,7,8-tetrahydro-2-naphthyl)-2,3-dihydro-1H-benzoimidazole-5-carboxylic Acid (**6d**).* To a solution of **16d** (120 mg, 0.30 mmol) in MeOH (10 mL) was added 2 N NaOH (10 mL). The reaction mixture was stirred at 60 °C for 30 min, poured into 1 N HCl (20 mL), and extracted with EtOAc (2 × 30 mL). The organic layer was washed with H_2O (40 mL) and brine (30 mL), dried over $MgSO_4$, and evaporated under reduced pressure to yield 110 mg of **6d** as a pale yellow solid (qy). The residue was recrystallized from EtOAc/*n*-hexane to yield 45 mg of **6d** as a colorless powder. Mp: > 295 °C; ^{1}H NMR (300 MHz, DMSO-d_6) δ: 12.69 (br s, 1H), 11.29 (s, 1H), 7.64 (dd, J = 8.0, 1.5 Hz, 1H), 7.59 (d, J = 1.5 Hz, 1H), 7.39 (s, 1H), 7.26 (s, 1H), 6.63 (d, J = 8.0 Hz, 1H), 2.01 (s, 3H), 1.68 (s, 4H), 1.31 (s, 3H), 1.30 (s, 3H), 1.24 (s, 3H), 1.23 (s, 3H); IR (KBr): 2959–2926 (OH), 1712 (CO), 1685 (CO) cm^{-1}. FAB-MS m/z: 379 $[M + H]^+$. Anal. Calcd for $C_{23}H_{26}N_2O_3 \cdot 1/4H_2O$: C, 72.13; H, 6.97; N, 7.31. Found: C, 72.40; H, 7.05; N, 7.18.

*1-(3,5,5,8,8-Pentamethyl-5,6,7,8-tetrahydro-2-naphthyl)-2-thioxo-2,3-dihydro-1H-benzoimidazole-5-carboxylic Acid (**6e**).* To a solution of **16e** (120 mg, 0.30 mmol) in MeOH (3.0 mL) was added 2 N NaOH (3.0 mL). The reaction mixture was stirred at 60 °C for 15 min, poured into 2 N HCl (30 mL), and extracted with EtOAc (2 × 20 mL). The organic layer was washed with H_2O (2 × 30 mL) and brine (30 mL), dried over $MgSO_4$, and evaporated under reduced pressure to yield 100 mg of **6e** as a pale yellow solid (86%). The residue was recrystallized from EtOAc/*n*-hexane to yield 90 mg of **6e** as pale yellow needles. Mp: > 295.0 °C. ^{1}H NMR (300 MHz, DMSO-d_6) δ: 13.20 (br s, 1H), 12.91 (br s, 1H), 7.76 (dd, J = 8.5, 1.5 Hz, 1H), 7.75 (d, J = 1.5 Hz, 1H), 7.41 (s, 1H), 7.24 (s, 1H), 6.68 (d, J = 8.5 Hz, 1H), 1.95 (s, 3H), 1.68 (s, 4H), 1.33 (s, 3H), 1.32 (s, 3H), 1.23 (s, 3H), 1.23 (s, 3H). IR (KBr): 3056 (NH), 2962–2923 (OH), 1693 (CO) cm^{-1}. FAB-MS m/z: 395 $[M + H]^+$. Anal. Calcd for $C_{23}H_{26}N_2O_2S \cdot 1/2H_2O$: C, 68.48; H, 6.74; N, 6.94. Found: C, 68.39; H, 6.63; N, 6.82.

*1-(3,5,5,8,8-Pentamethyl-5,6,7,8-tetrahydronaphthalen-2-yl)-1H-indole-5-carboxylic Acid Methyl Ester (**19**).* To a solution of **17** (1.0 g, 3.6 mmol) and **18** (530 mg, 3.0 mmol) in dry toluene (4.0 mL) were added CuI (28 mg, 0.15 mmol), K_3PO_4 (1.3 g, 6.3 mmol), KI (600 mg, 3.6 mmol), and *N*,*N*′-dimethylethylenediamine (65 μL, 0.60 mmol). The reaction mixture was refluxed at 160 °C for 2.5 h under microwave irradiation, filtered through Celite, and evaporated

dx.doi.org/10.1021/jm400033f | J. Med. Chem. 2013, 56, 1865–1877